Proceedings of the Seventh International Conference on
Railway Technology: Research, Development and Maintenance
Edited by: J. Pombo
Civil-Comp Conferences, Volume 15, Paper 16.6
Civil-Comp Press, Edinburgh, United Kingdom, 2026
ISSN: 2753-3239, doi: 10.4203/ccc.15.16.6

Simulation and Experimental Validation of a Locomotive-Based Weighing System for Industrial Sidings

A. Von Stillfried and R. Pfaff

Institute for Rail Vehicles (IFS), RWTH Aachen University, Germany

Abstract

Accurate knowledge of freight wagon mass is essential for safe railway operation and reliable billing in industrial siding logistics. Existing weighing methods typically require dedicated track-scale infrastructure or wagon-mounted sensor systems, which can involve substantial investment or limited applicability. This paper presents an infrastructure-independent weighing concept in which a measurement system installed on a shunting road-rail vehicle estimates wagon mass from the coupling force and vehicle acceleration with linear regression on filtered measurement data. A multibody simulation model of a road-rail vehicle coupled to an Eanos freight wagon was developed to evaluate the influence of different conditions. Simulation results showed measurement deviations of approximately ± 4 % under operational conditions. Real-world tests demonstrated good repeatability, with 80 % of measurements errors by less than 2 % or 360 kg from the mean measured mass. The results indicate that locomotive-based freight wagon weighing is technically feasible and promising for cost-effective industrial siding applications, although further validation with different freight wagon types and loading conditions is required to improve absolute accuracy.

Keywords: freight wagon, weighing, multibody simulation, road-rail vehicle, industrial siding, dynamics, simulation-to-reality transfer, data analysis

1 Introduction

Knowledge of the weight of freight wagons entering and leaving a railway siding is necessary both to ensure safe railway operations and to monitor the flow of goods and the associated cost settlements. To ensure the safe operation of railways, it is necessary to determine the braking performance of trains according to the EN 16834 standard [1]. The EN 15528 standard defines route classes, each of which has a maximum axle load and maximum load per unit of length [2]. These must be taken into account when planning a journey. Furthermore, the freight wagon must not be loaded beyond its maximum weight. For companies with railway sidings to operate cost-effectively, it is essential to know the exact weight of incoming and outgoing goods in order to issue the relevant invoices or check delivery notes. Relevant documents in this area are the 'General Contract of Use for Wagons' and the 'Uniform Rules Concerning the Contract of International Carriage of Goods by Rail' [3, 4].

At present, weighing is mainly carried out using the following methods:

- Track scales: The weighing process can take place whilst the vehicle is stationary or whilst it is moving slowly across the weighbridge. Weighing whilst stationary is carried out on non-autonomous weighbridges, which are subject to EU Directive 2014/31/EU [5]. In this process, a section of track is isolated from the rest of the track infrastructure and supported on load cells, which record the weight of the vehicle. To be weighed, the vehicle must be stationary on the weighing track and, where necessary, uncoupled from other wagons [6]. In practice, accuracies of 0.2 % are achieved [7]. Weighing during passage is carried out on automatic weighbridges in accordance with EU Directive 2014/32/EU [8]. In most cases, strain gauges are fitted to the rails or load cells are installed between the rail and the sleeper. Systems are available with a passage speed of $v = 30~\frac{\mathrm{km}}{\mathrm{h}}$ [9].

- On-board systems: In addition to measurement technology installed in the infrastructure, it is also possible to fit the freight wagons themselves with sensors to determine their weight. As part of the digitalisation of freight wagons for the real-time monitoring of vehicle fleets, sensors capable of determining weight are increasingly being installed [10]. The systems are also used to warn of overloading during loading [11].

- Weighing during loading: If there is no infrastructure in place for weighing goods wagons, the weight of general cargo can be determined during loading. If, for example, the weight of individual pallets is known, these can be added together.

The methods currently used for weighing freight wagons all have in common that they either entail a significant investment in infrastructure or the retrofitting of entire fleets of wagons, or they depend on the type of goods to be loaded. This situation has given rise to the motivation to develop a cost-effective weighing system that is installed on the shunting locomotive and is therefore not dependent on infrastructure or freight wagon equipment.

2 Concept

Whilst a freight wagon is in motion, various forms of resistance arise that counteract its forward movement, such as rolling resistance, aerodynamic drag and gradient resistance [12]. These forms of resistance depend on both external factors and the wagon's own characteristics, such as its mass, condition and shape. The resistances can be grouped in various ways. In the following, an acceleration-dependent term $R_a(a)$ and an acceleration-independent term R_{rest} are introduced:

$$\sum R_{\text{wag}} = R_a(a) + R_{\text{rest}} \tag{1}$$

R_a consists primarily of the longitudinal mass inertia and rotation mass inertia, so the sum of the resistances $\sum R_{\text{wag}}$ can be determined as

$$\sum R_{\text{wag}} = (m_{\text{fw}} + m_{\text{fw,rot}}) \cdot a + R_{\text{rest}} \tag{2}$$

As all resistance is transmitted via the vehicle coupling, $\sum R_{\text{wag}}$ can be determine as

$$\sum R_{\text{wag}} = F_{\text{coup}} \tag{3}$$

so the weight of the carriage can be estimated by measuring the coupling force F_{coup} and the acceleration of the locomotive. By using a large number of data points, a linear regression can be performed and both the term $m_{\text{fw}} + m_{\text{fw,rot}})$ and R_{rest} can be determined. The application of a filter to the data prior to analysis, with the objective of removing artefacts and data points characterised by low acceleration or force values can further improve the result. As the rotational mass in a conventional freight wagon consists mainly of the wheels, the average rotational mass of a wheelset $m_{\text{rot,ws}} =$ 288 kg is subtracted from the result, multiplied by the number of wheelsets, following the regression analysis. If only a difference measurement is taken (before and after loading or unloading), this step can be omitted.

3 Simulation

A multi-body simulation model was developed to investigate the influence of various disturbance factors during a measurement.

3.1 Modelling

A 'Rotrac E2' road-rail vehicle manufactured by G. Zwiehoff GmbH, with a maximum towing capacity of $m_{\text{tow,max}} = 250$ t, is used as the locomotive. A 'Eanos' freight wagon, a four-axle open freight wagon for bulk goods with a length of $l_{\text{Eanos}} = 14.5$ m without buffers, is coupled to this vehicle, see Figure 1 [13].

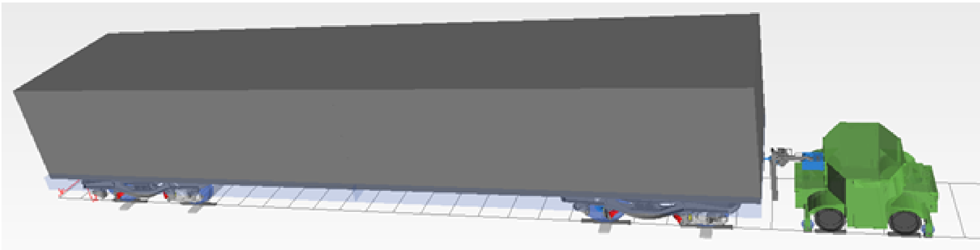

Figure 1: Simulation model of Rotrac E2 an Eanos freight wagon

The condition of the freight wagon is modelled by variations in wheel radius ($r_{\text{new}} = 0.46$ m; $r_{\text{worn}} = 0.42$ m), the occurrence of flat spots up to a length of $l_{\text{flatspot,max}} = 80$ mm, and variations in the rolling resistance coefficient, which can range from $f_{\text{r,min}} = 0.0005$ to $f_{\text{r,max}} = 0.0062$ during shunting operation [14]. The coupling is simulated as a UIC screw coupling with side buffers according to UIC-Leaflet 520 [15].

The road-rail vehicle is modelled according to the vehicle data [16]. The traction force is transmitted through the rubber wheels, while steel wheels ensure the track guiding. The coupling is an automatic shunting coupling, through which both buff and draft forces are transmitted via the central bar and the draw hook of the freight wagon.

The route is modelled on a fictional railway siding is based on an example in [17], as shown in figure 2. Empty wagons are standing ready on track 2, to be loaded individually at the loading point. The loaded wagons are to be parked on track 1. The road-rail vehicle pulls one wagon at a time from track 2 to the loading point, where a mass – chosen at random for this experiment – is added to it. Since the road-rail vehicle does not change sides while loading, the wagon is then pushed onto track 1. The route from track 2 to the loading point consists initially of a straight track, the length of which depends on the starting position of the road-rail vehicle. This is followed by a left-hand and a right-hand curve, each with $r_{\text{track}} = 180$ m and $l_{\text{curve}} = 30$ m, without a transition curve. The second curve represents switch 3 (S3 in figure 2) in the branch position. The loading point is located immediately behind switch 3. The route from the loading point to track 1 consists solely of a continuous straight section, which also includes the straight section of switch 3. There are no longitudinal gradients. The tracks exhibit track alignment defects. They are classified as 'good' to 'average' track alignment according to [18]. This means that with the power spectral density

$$\Theta = \frac{a}{(b + \frac{\Omega}{2\pi})^3} \tag{4}$$

the track alignment is modelled the the unevenness a and waviness b shown in table 1.

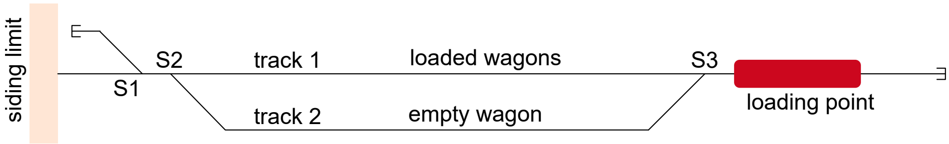

Figure 2: Modelled siding

Irregularity	Unevenness a [m^2]	Waviness b [1/m]
vertical alignment h	$2.44 \cdot 10^{-9}$	$1.31 \cdot 10^{-2}$
lateral alignment u	$2.84 \cdot 10^{-9}$	$1.48 \cdot 10^{-2}$
track gauge s	$1.83 \cdot 10^{-8}$	$1.06 \cdot 10^{-2}$
cross level angle δ	$8.36 \cdot 10^{-16}$	$5.56 \cdot 10^{-3}$

Table 1: Uneveness and waviness used for siding modelling

3.2 Test procedure

In a simulation run, following a 'settling time' of $t_{\text{sim}} = 1$ s, during which the models can respond to the specified conditions, the train is accelerated until it reaches a speed of $v_{\text{target}} = 1\ \frac{\text{m}}{\text{s}}$. This is followed by a coasting phase at a constant speed until the loading point is reached. A PID controller regulates the drive power of the road-rail vehicle during this phase. Once the loading point has been reached, the train is braked to a standstill again. The return journey with the loaded freight wagon is carried out in the same way. Since the road-rail vehicle does not run around the train, the goods wagon is pushed in this case. The simulation is carried out in a SIMPACK-SIMULINK co-simulation, in which SIMPACK executes the multi body simulation and SIMULINK controls the traction force of the road-rail vehicle. The data analysis is carried out as described in section 2. Only data points from the acceleration phase and deceleration phase were used. Figure 3 shows the data points and the data analysis for a measurement taken during a journey from the loading point to track 1. The large number of data points with a force $F_{\text{coup}} = 0$ kN indicates that, at the start of acceleration and during the transition from acceleration to braking, the coupling is travelling through its free play, meaning that no force is being transmitted. The slope of the regression line represents the measured mass. It can be seen that considering both the acceleration (positive acceleration and force values) and braking phases (negative acceleration and force values) together makes the linear regression significantly more robust and therefore more accurate.

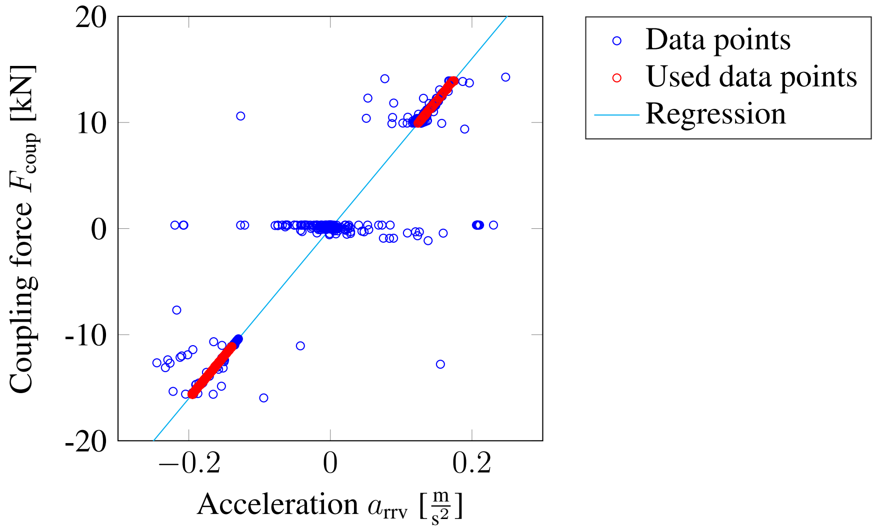

Figure 3: Linear regression based on simulated measurement data

3.3 Results

Figure 4 shows the results of 1,024 different simulation runs. Figure 4 (a) plots the relative measurement error

$$\chi = \frac{m_{\text{measured}} - m_{\text{real}}}{m_{\text{real}}} \tag{5}$$

of the measurements taken during the journey from track 2 to the loading point against the mass to be loaded following that journey. As all wagons are empty here, the only variables are the condition of the goods wagon and the wind conditions. This results in measurement uncertainties of $\chi = \pm 4\ \%$. Figure 4 (b) shows the measurement results for the return journey from the loading point to track 1. The measurement error decreases as the mass increases, from $\chi_{m_{\text{pl}}=0} \approx 3\ \%$ to $\chi_{m_{\text{pl}}=max} \approx 0.5\ \%$. The difference in mass resulting from these two measurements is shown in Figure 4 (c). It can be seen that, particularly for small payloads, these can only be determined with comparatively high relative measurement deviations. For large payloads, these are determined much more accurately, with a relative measurement error of $\chi \approx 0.01$.

This behaviour is due to the definition of χ given by equation 5. In Figure 4 (d), the absolute mass deviation Δm_{fw} is therefore plotted against the mass of the load. The absolute difference remains relatively constant across the range of load masses. The $90\ \%$ and $100\ \%$ limits indicate the permissible measurement error for a automatic weigh-in-motion system in class 2 according to OIML R 106-1, the standard for automatic weigh-in-motion systems, for a vehicle with a maximum weight of $m_{\mathrm{max}} = 90$ t [19]. These limits do not apply explicitly to difference measurements, but they do provide an indication of the actual accuracy. It shows that almost all measured values lie below the $90\ \%$ limit and therefore meet the requirements of this accuracy class. Figure 5 shows histograms of the relative and absolute measurement deviations. The mean of the relative measurement deviation is $\bar{\chi} = -0.0101$ with a standard deviation of $\sigma_{\chi} = 0.0198$. The mean absolute measurement uncertainty is $\Delta\bar{m}_{\mathrm{fw}} = -111.19$ kg with a standard deviation of $\sigma_{\Delta m_{\mathrm{fw}}} = 209.46$ kg.

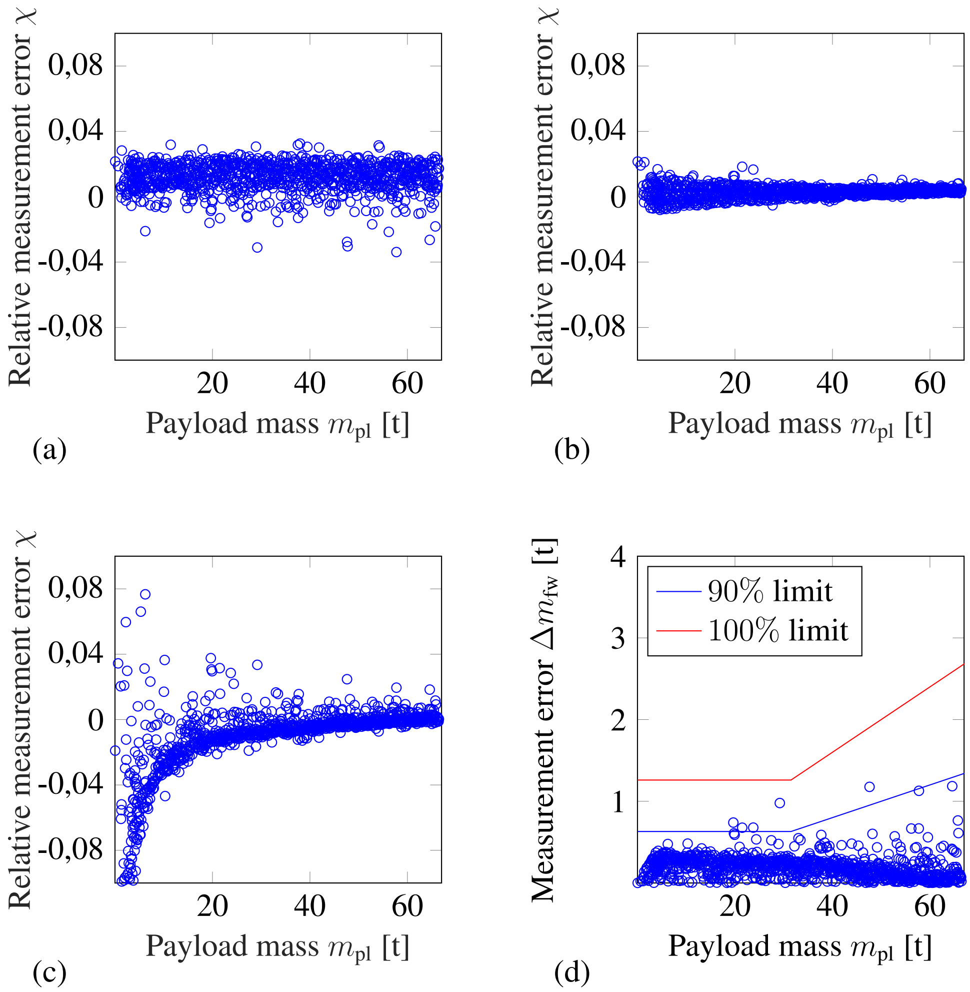

Figure 4: Simulation results of a siding operation ($N = 1024$)

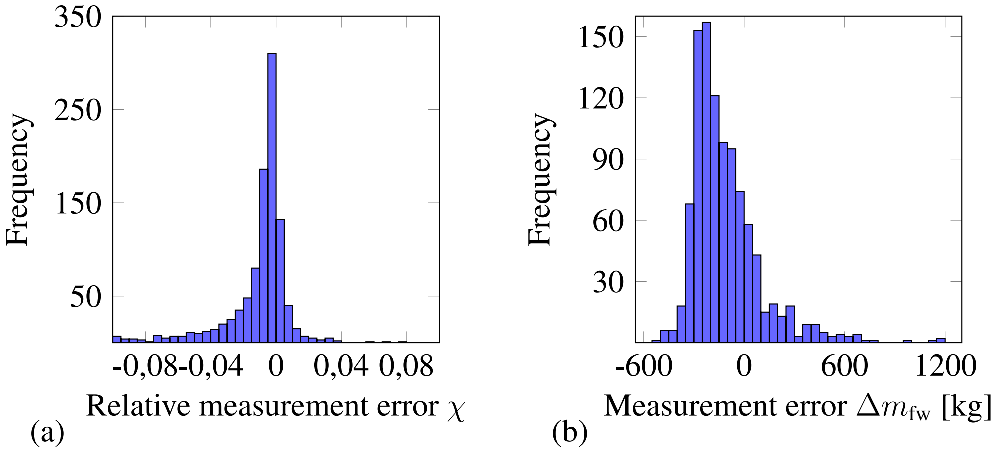

Figure 5: Accuracy of the simulation of siding operation ($N = 1024$)

4 Experiments

In order to validate the concept presented and used in the simulation against real measurement data, a measurement system was developed and installed in a road-rail vehicle 'Rotrac E2'. A load cell with a nominal force of $F_{\text{nom}} = 100\ kN$ is installed between the head and the shaft of the shunting coupling. Figure 6 shows the load cell mounted with adapter plates in the shunting coupling. The acceleration is measured with a capacitive acceleration sensor with an maximum acceleration of $a_{\text{max}} = \pm 2g$. A digital measurement amplifier reads the sensors and stores the data.

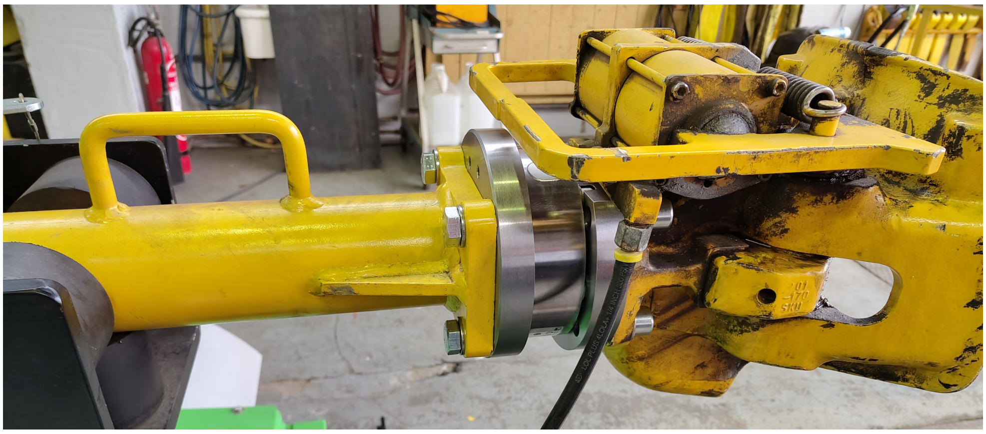

Figure 6: Mounted load cell in shunting coupling

For the experiments, a 'Köf' shunting locomotive was coupled to the road-rail vehicle instead of a goods wagon, see Figure 7. Each experiment consists of an acceleration phase, a short coasting phase and subsequent braking to a standstill. During a measurement, a distance of $s \approx 6$ m is covered. A total of $N = 100$ measurements were carried out, of which 50 involved the locomotive being pulled and 50 involved it being pushed.

Figure 7: Experiment setup consisting of shunting locomotive Köf and road-rail vehicle Rotrac E2

Data analysis is generally carried out using the method described in Section 2, involving data filtering followed by linear regression. However, for this set of measurement data, the selection of the data points used for the linear regression is carried out using a second, preliminary linear regression. This is fitted to all the recorded data points. Subsequently, all data points where the coupling force deviates by more than $50\ \%$ from the determined straight line are filtered out. The second linear regression is then fitted to the remaining data points.

Figure 8 shows the recorded data points and the two-stage linear regression of a measurement. Compared with Figure 3, it can be seen that the large number of measurement points with a coupling force $F_{\text{coup}} = 0$ kN is also present. Here, as shown in the simulation, the free play of the coupling is traversed. The remaining measurement points are distributed along the linear regression line, alongside the outliers that are also present, with the measurement points being more evenly distributed over the x-axis than in the simulation. This is due to the different driving behaviour of the test vehicle. Whilst the simulation employs a simplified driving style with constant maximum drive torque, real-world measurements involve a 'smoother' acceleration and deceleration.

Figure 9 (a) shows a histogram of the frequency of the relative measurement error χ and the absolute measurement error for the individual measurements. The reference value $m_{\text{mean}} = 16.29$ t is the mean of all the masses determined, which is not to be equated with the actual mass ($m_{\text{Köf}} = 17$ t). Individual measurements deviate from the mean by up to $\chi = 5\ \%$ or $\Delta m = 900$ kg. Figure 9 (b) shows the cumulative frequency of the measurement errors. It can be seen that 80 % of the measurements deviate by less than $\chi = 2\ \%$ or $\Delta m = 360$ kg from the mean. The standard deviation of the measured masses is $\sigma_\chi = 0.013$ and $\sigma_{\Delta m} = 208.83$ kg respectively.

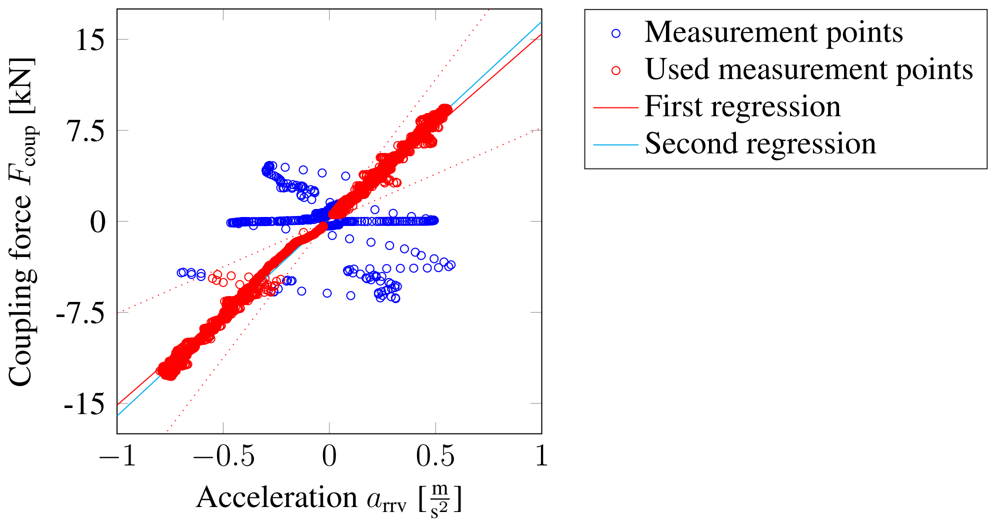

Figure 8: Two-stage linear regression based on real measurement data

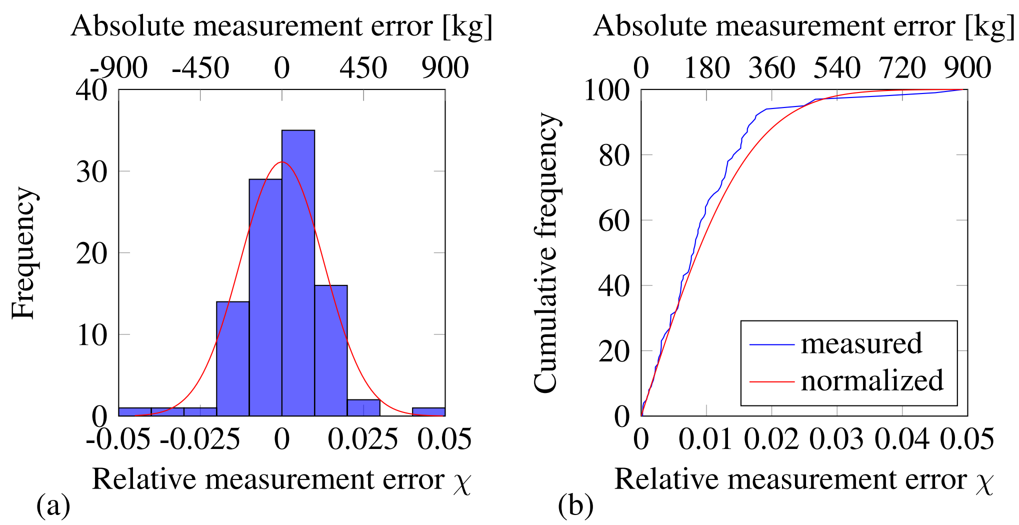

Figure 9: Distribution function and cumulative distribution function of 100 measurements

Despite satisfactory repeatability, there remains a 4 % discrepancy between the measured mass and the actual mass. This may be because the stated weight of the locomotive $m_{\text{Köf}} = 17$ t is incorrect. This value is based on vehicle data; it was not possible to weigh the locomotive independently. A second reason may be that the sensors have been calibrated incorrectly. In further experiments, these errors can be addressed and the measurement accuracy further improved. However, the measurement data show that the concept works in principle and that further development looks promising.

5 Conclusion

This paper presents an innovative approach to weighing freight wagons, which is independent of the infrastructure and the equipment fitted to the wagons. The concept is based on measuring the coupling force during acceleration of the shunting locomotive and is installed on the locomotive itself. A multi-body simulation using a road-rail vehicle as the shunting locomotive and an Eanos freight wagon demonstrated that measurement accuracies of 4 % can be achieved in operational conditions and that the regulatory requirements for weigh-in-motion systems can be met. Real-world measurements using a shunting locomotive as a freight wagon and a road-rail vehicle have shown that the repeatability is around 2 %. In order to further develop the system and the data analysis, the next steps could involve expanding the simulation to include additional influencing factors and various types of freight wagons, and recording real-world measurement data from freight wagons in different loading conditions.

References

[1] *DIN EN 16834 Railway applications - Braking - Brake performance*, Jul. 2019. DOI: 10.31030/2811676.

[2] *DIN EN 15528 Railway applications - Line categories for managing the interface between load limits of vehicles and infrastructure*, Feb. 2022. DOI: 10.31030/3264066.

[3] "Contract – GCU." (), [Online]. Available: https://gcubureau.org/contract/ (visited on 03/24/2026).

[4] *Uniform Rules concerning the Contract of International Carriage of Goods by Rail (CIM - Appendix B to the Convention)*, 1999. [Online]. Available: https://otif.org/de/?page_id=172.

[5] Official Journal of the European Union, *Directive 2014/31/EU of the European Parliament and of the Council of 26 February 2014 on the harmonisation of the laws of the Member States relating to the making available on the market of non-automatic weighing instruments*.

[6] M. Kochsiek, Ed., *Handbuch des Wägens*, Braunschweig: Vieweg, 1989, ISBN: 3-528-18572-4.

[7] U. Bitzer, “Genauigkeit von industriellen Wiegesystemen,” *Mühle + Mischfutter*, no. 18, 2009.

[8] Official Journal of the European Union, *Directive 2014/32/EU of the European Parliament and of the Council of 26 February 2014 on the harmonisation of the laws of the Member States relating to the making available on the market of measuring instruments*.

[9] “DYNARAIL - Dynamische Gleiswaage eichfähig,” Hastema. (), [Online]. Available: `https://www.hastema.com/de/portfolio-posts/dynarail-dynamische-gleiswaage-eichfaehig/` (visited on 12/03/2025).

[10] J. Janicki, H. Reinhard, and M. Rüffer, *Schienenfahrzeugtechnik* (DB-Fachbuch), 4. Auflage. Berlin: Bahn Fachverlag, 2020, ISBN: 978-3-943214-26-0.

[11] PJ Monitoring GmbH, *Loading made easy with the digital freight train*. [Online]. Available: `https://pjm.co.at/waggontracker/` (visited on 01/29/2026).

[12] S. Iwnicki, M. Spiryagin, C. Cole, and T. McSweeney, Eds., *Handbook of Railway Vehicle Dynamics, Second Edition*, 2nd ed., Boca Raton: CRC Press, Nov. 14, 2019, 913 pp., ISBN: 978-0-429-46939-8. DOI: `10.1201/9780429469398`.

[13] “Eanos-x 056,” DB Cargo Güterwagenkatalog. (2025), [Online]. Available: `https://gueterwagenkatalog.dbcargo.com/katalog/nach-gattung/e-offene-wagen/Eanos-x-056-5831764` (visited on 10/13/2025).

[14] M. Scheuch, “Zum Stand der Laufzielbremsung in Ablaufanlagen und ihr Beitrag zur Industrie 4.0,” *Signal+Draht*, vol. 03/2020, pp. 17–22, Mar. 2020.

[15] *UIC Leaflet 520: Wagon, choaches and vans - Draw gear - Standardisation*, Dec. 2003.

[16] G. Zwiehoff GmbH, Ed., *Brochure Rotrac E2*, 2025.

[17] H.-S. Jung, “Bedarfsgerechtes Flachrangieren mit einem autonomen Zweiwege-Rangiergerät,” Ph.D. dissertation, RWTH Aachen University, Aachen, 2025, 160 pp.

[18] F. Frederich, “Die Gleislage - aus fahrzeugtechnischer Sicht,” *ZEV Glasers Annalen*, vol. 108, no. 12, pp. 355–361, 1984, ISSN: 1618-8330.

[19] *OIML R 106-1: Automatic rail-weighbridges Part 1: Metrological and technical requirements - Tests*, 2011.